

1 Ciliary ARL13B is essential for body weight regulation in adult mice
2
3

4 Tiffany T. Terry^a, Eduardo D. Gigante^{a, b, c}, Coralie M. Alexandre^d, Kathryn M. Brewer^e, Xinyu
5 Yue^d, Nicolas F. Berbari^e, Christian Vaisse^d, Tamara Caspary^{a, f}
6
7

8 ^a Department of Human Genetics, Emory University School of Medicine, Atlanta, GA, 30322
9

10 ^b Graduate Program in Neuroscience, Laney Graduate School, Emory University, Atlanta, GA,
11 30322

12 ^c Present address: Department of Molecular and Cellular Biology, Kennesaw State University,
13 Kennesaw, GA, 30144

14 ^d Diabetes Center and Department of Medicine, University of California, San Francisco, San
15 Francisco, CA, 94143

16 ^e Department of Biology, Indiana University- Indianapolis, Indianapolis, IN, 46202

17 ^f Address correspondence to: Tamara Caspary (tcaspar@emory.edu), 404-727-9862

18 ORCID and email for authors:

19 Tiffany T. Terry 0000-0002-2729-6281, tiffany.terry@emory.edu

20 Eduardo D. Gigante 0000-0002-1486-5377, egigante@kennesaw.edu

21 Coralie M. Alexander 0009-0004-2978-2648 Coralie.Alexandre@ucsf.edu

22 Kathryn M. Brewer 0009-0006-3498-4492 katmbrew@iu.edu

23 Xinyu Yue 0000-0002-6187-5906 Xinyu.Yue@ucsf.edu

24 Nicolas F. Berbari 0000-0003-2863-1069 nberbari@iu.edu

25 Christian Vaisse 0000-0003-4274-7033 Christian.Vaisse@ucsf.edu

26 Tamara Caspary 0000-0002-6579-7589, tcaspar@emory.edu

27

28

29

30

31

32

33

34

35

36 **Abstract**

37 Cilia are near ubiquitous cellular appendages critical for cell-to-cell communication and involved
38 in diverse developmental and homeostatic processes. ARL13B is a regulatory GTPase enriched
39 in cilia. We engineered an *Arl13b* mouse allele, *Arl13b*^{V358A}, which retains ARL13B biochemical
40 activities but renders ARL13B undetectable in cilia. Surprisingly, these mice are hyperphagic
41 and become obese and insulin resistant. In addition to its GTPase function, ARL13B acts as a
42 guanine nucleotide exchange factor (GEF) for ARL3. To test whether ARL13B's GEF activity is
43 required to regulate body weight, we analyzed the body weight of mice expressing an ARL13B
44 variant lacking ARL3 GEF activity (*Arl13b*^{R79Q}). We found no difference in body weight,
45 indicating ARL13B is unlikely to regulate weight via its ARL3 GEF activity. Ciliary ARL13B could
46 control energy homeostasis through a role in development or in adult mice. We induced wildtype
47 ARL13B expression, which localizes to cilia, in 4-week-old *Arl13b*^{V358A/V358A} mice and found the
48 obesity phenotype and associated metabolic impairments were rescued, consistent with
49 ARL13B regulating homeostatic signaling within cilia in adult mice. These results show that
50 ciliary ARL13B functions to control body weight. Our ability to genetically control the subcellular
51 localization of ARL13B by removing and introducing it into cilia enables us to define the cilia-
52 specific role of ARL13B and provides key information for understanding how cilia act as a
53 signaling hub critical for energy homeostasis.

54 **Author Summary**

55 Primary cilia are essential for energy homeostasis, and their disruption leads to syndromic
56 obesity. However, the mechanisms by which ciliary components regulate energy balance
57 remain unclear. Here, we identify a key role for the ciliary GTPase ARL13B in energy
58 homeostasis. Using a mouse model expressing the ARL13B^{V358A} variant, which is excluded from
59 cilia but retains biochemical activity, we show that ciliary ARL13B regulates body weight, as
60 *Arl13b*^{V358A/V358A} mice become obese and hyperphagic. Remarkably, restoring ciliary ARL13B in

61 these mice rescues obesity, demonstrating its crucial role in acute ciliary signaling for energy
62 balance. This study directly links ciliary ARL13B with energy balance in adult animals.

63

64 **Introduction**

65 *Ar13b*, an ADP-ribosylation factor (ARF) protein family member, encodes a regulatory
66 GTPase highly enriched on the ciliary membrane^(1, 2). Like other regulatory GTPases, ARL13B
67 has multiple functions, likely mediated by distinct effectors. For example, it has a conserved role
68 as a guanine nucleotide exchange factor (GEF) for ARL3^(3, 4). In cilia, ARL13B regulates
69 retrograde intraflagellar transport as well as the phospholipid composition of the ciliary
70 membrane⁽⁵⁻⁷⁾. In mice, loss of ARL13B is embryonic lethal, disrupting ciliogenesis and
71 Hedgehog (Hh) signaling^(8, 9). Patient mutations in *ARL13B* cause the ciliopathy Joubert
72 Syndrome (JS)^(10, 11). JS patients present with developmental delay, intellectual disability, and
73 physical anomalies, and all known causative *ARL13B* mutations disrupt ARL13B's GEF activity
74 for ARL3⁽⁴⁾.

75 We engineered an ARL13B mouse variant (ARL13B^{V358A}) that maintains the known
76 biochemical functions of ARL13B but is undetectable in cilia⁽¹²⁾. Surprisingly, these mice display
77 normal Hh signaling but retain the ciliogenesis defects seen in the null allele⁽¹²⁾. These data
78 argue that cellular ARL13B regulates Hh, and ciliary ARL13B controls ciliogenesis. Thus,
79 homozygous *Ar13b*^{V358A/V358A} mice (hereafter called *Ar13b*^{A/A}) reveal ciliary ARL13B function,
80 after embryonic development and in adult animals.

81 Outside of JS, several other ciliopathies cause metabolic abnormalities and obesity.
82 Alstroem (ALMS) syndrome and Bardet-Biedl syndrome (BBS) are among the ciliopathies in
83 which obesity is a major clinical feature⁽¹³⁻¹⁵⁾. For example, loss of function mutations in *ALMS1*
84 lead to defects in cilia assembly and function, impacting ciliation and ciliary signaling in cells that

85 regulate appetite and energy balance⁽¹⁶⁻¹⁸⁾. BBS mutations disrupt cilia protein import and
86 export, impacting ciliary signaling and trafficking of proteins involved in regulating food intake
87 and energy metabolism⁽¹⁹⁻²²⁾. In adult mice, genetic ablation of cilia causes obesity due to
88 hyperphagia and leads to elevated levels of leptin, glucose, and insulin^(23, 24). Loss of cilia on
89 specific neuronal cell types during development also results in hyperphagia-associated
90 obesity^(23, 25, 26). Together, these findings show that primary cilia are required for regulating
91 energy homeostasis. Yet, these approaches have been unable to distinguish the cilia-specific
92 roles of proteins compared to their functions in other parts of the cell. Understanding the role of
93 cilia-mediated signaling in obesity will likely uncover mechanisms driving common forms of
94 obesity.

95 Here, we report that *Arl13b*^{A/A} mice become hyperphagic and obese, indicating that the
96 cilia-specific function of ARL13B is critical for energy homeostasis regulation. ARL13B's GEF
97 activity for ARL3 is unlikely to be required to regulate body weight as mice expressing a variant
98 (*Arl13b*^{R79Q}) that lacks *in vitro* ARL13B GEF activity for ARL3 are not overweight. Rescuing
99 ciliary ARL13B in 4-week-old *Arl13b*^{A/A} mice prevents obesity, suggesting ARL13B controls
100 body weight through a homeostatic role in ciliary signaling. These findings demonstrate that
101 ciliary ARL13B is essential for body weight regulation in adult mice and provides a molecular
102 entry point for understanding the complex roles ciliary signaling plays in adult energy
103 homeostasis.

104

105 **Results**

106 ***ARL13B*^{V358A} protein is undetectable in primary cilia in adult mouse tissues**

107 The engineered ARL13B^{V358A} variant disrupts ARL13B from localizing to primary cilia in
108 mouse embryonic fibroblasts, neural tube, and kidneys^(12, 27, 28) (**Figure 1 A and B**). To assess

109 whether ARL13B^{V358A} protein is in cilia in cell types previously implicated in ciliopathy-associated
110 metabolic phenotypes, we performed immunofluorescence staining for ARL13B and the
111 neuronal cilia marker adenylate cyclase 3 (ADCY3) in the hypothalamus and endocrine
112 pancreas^(29, 30). In the hypothalamus, we detected ADCY3 staining in the arcuate (ARC), the
113 paraventricular (PVN), and the ventromedial (VMH) hypothalamic nuclei, indicating the
114 presence of neuronal cilia. In control mice, ARL13B co-localizes with ADCY3 in the ARC, the
115 PVN, and VMH, indicating it is normally present in cilia (**Figure 1 C, E, G**). However, we could
116 not detect the ARL13B signal in neuronal cilia in these brain regions of *Ar13b^{A/A}* mice, indicating
117 the engineered variant does not enrich in these cilia (**Figure 1 D, F, H**). In the ARC, appetite-
118 stimulating agouti-related peptide (AgRP)-expressing neurons and the appetite-suppressing
119 pro-opiomelanocortin (POMC)-expressing neurons are key regulators of food intake⁽³¹⁾. To
120 assess whether loss of ciliary ARL13B disrupted the number or patterning of AgRP and POMC
121 neurons in the ARC, we performed RNAscope in situ hybridization. We found normal frequency
122 and patterning for both AgRP and POMC neurons in the ARC of *Ar13b^{A/A}* mice, indicating ciliary
123 ARL13B does not play a role in the hypothalamic patterning of these cell types (**Supplemental**
124 **Figure 1 A-D**).

125 To determine whether ARL13B^{V358A} protein is detectable on pancreatic islet cells, we
126 performed immunofluorescence staining for ARL13B, acetylated α -tubulin, glucagon (α -cells),
127 and insulin (β -cells). We observed ARL13B co-localizes with acetylated α -tubulin on α - and β -
128 cells in the cilia of control mice but not on pancreatic islet cells in *Ar13b^{A/A}* mice (**Supplemental**
129 **Figure 2 A-D**). These findings demonstrate that ciliary ARL13B is present in both the
130 hypothalamic feeding centers and pancreatic islets of adult mice, but in mice expressing the
131 ARL13B^{V358A} variant, ARL13B is undetectable in cilia.

132 ***Ar13b^{A/A} mice are obese, hyperphagic, and insulin-resistant***

133 Whereas the *Arl13b*^{hnn/hnn} null mice are embryonic lethal, homozygous *Arl13b*^{A/A} survive
134 into adulthood and display an increased body weight compared to wildtype (*Arl13b*^{+/+}) control
135 littermates⁽⁸⁾. To investigate their body weight profile, we generated longitudinal data from
136 weaning (week 3) to adult (week 10). We found no significant differences in body weight curves
137 among the control genotypes: *Arl13b*^{+/+}, *Arl13b*^{A/A}, and *Arl13b*^{+/hnn} in male and female mice,
138 indicating the mutations are recessive and display no evidence of a gain-of-function (e.g.
139 dominant negative) effect. The *Arl13b*^{A/A} mice became significantly heavier than all control
140 genotypes at week 5 for males and week 7 for females (**Figure 2 A and B**). By week 10, both
141 male and female *Arl13b*^{A/A} mice were, on average, 30% heavier than controls.

142 *Arl13b*^{A/A} mice are obese, as the increase in weight was exclusively attributed to an
143 increase in fat mass. Body composition analysis showed comparable lean mass between
144 *Arl13b*^{A/A} and control animals (**Figure 2 C and H**). The difference in body weight between the
145 two genotypes was characterized by a 123% increase in fat mass in male *Arl13b*^{A/A} mice and a
146 158% increase in fat mass in female *Arl13b*^{A/A} mice (**Figure 2 D and I**). Consistent with the
147 increase in fat mass, we also observed increased leptin levels in *Arl13b*^{A/A} mice (**Figure 2 E and**
148 **J**).

149 To evaluate whether the *Arl13b*^{A/A} weight phenotype is sensitive to *Arl13b* gene dosage,
150 we bred the *Arl13b*^A allele with the null *Arl13b*^{hnn} allele. We weighed male and female *Arl13b*^{A/hnn}
151 heterozygous mice from weeks 3 to 10. We found that *Arl13b*^{A/hnn} mice displayed a similar body
152 weight phenotype to *Arl13b*^{A/A} mice, indicating that less overall ARL13B protein had no impact
153 on this phenotype (**Figure 2 A and B**).

154 To examine whether the obesity phenotype is the result of changes in feeding, we
155 measured food intake from weeks 4 to 5, just prior to when we first observed an increase in
156 *Arl13b*^{A/A} body weight. We found that male and female *Arl13b*^{A/A} mice consumed, on average,
157 ~20% more food per day compared to littermate controls (**Figure 2 F and K**). To investigate
158 whether changes in activity and/or metabolism contribute to the increased body weight in

159 *Arl13b*^{A/A} mice, we measured energy expenditure using a Comprehensive Lab Animal
160 Monitoring System (CLAMS). Male *Arl13b*^{A/A} mice displayed a modest 13% increase in daily
161 energy expenditure (**Figure 2G**). Females showed no changes in energy expenditure compared
162 to control animals (**Figure 2L**). These data demonstrate that the increase in body weight we
163 observe in male and female *Arl13b*^{A/A} mice is due to hyperphagia.

164 We further determined whether excluding ARL13B from cilia influenced glycemic
165 regulation. *Arl13b*^{A/A} mice were hyperinsulinemic (**Figure 3 A and B**) and normoglycemic
166 (**Figure 3 C-F**) at baseline, suggesting conserved insulin production by beta-cells. During
167 glucose tolerance tests, both male and female *Arl13b*^{A/A} mice exhibited elevated blood glucose
168 levels, but these were only significant in females (**Figure 3 C and D**). Insulin did not lower blood
169 glucose levels in male and female *Arl13b*^{A/A} mice compared to controls, revealing an insulin-
170 resistance phenotype consistent with the changes we observed in body composition (**Figure 3**
171 **E and F**). Together, these data indicate that *Arl13b*^{A/A} mice are hyperinsulinemic, glucose
172 intolerant, and insulin resistant, congruent with their obese phenotype.

173

174 ***ARL13B's GEF activity for ARL3 does not appear to regulate energy homeostasis***

175 One possible mechanism of ARL13B action within cilia is via its GEF activity for ARL3,
176 which would imply that activated ARL3 is involved in energy homeostasis regulation^(3, 4, 32, 33).
177 This predicts that the obesity we observed upon restricting ARL13B from cilia in *Arl13b*^{A/A} mice
178 would be recapitulated by disrupting ARL13B's function via its GEF activity for ARL3. To test
179 this directly, we examined mice in which we modified the endogenous *Arl13b* locus to express
180 only the ARL13B variant *Arl13b*^{R79Q}, which lacks *in vitro* GEF activity for ARL3^(4, 34) (**Figure 1A**).
181 We found that *Arl13b*^{R79Q/R79Q} mice displayed normal body weight (**Figure 4 A and B**). While we
182 cannot exclude the possibility of a compensatory GEF for ARL3, these findings suggest that the
183 obesity phenotype in *Arl13b*^{A/A} mice is likely independent of ARL13B's GEF activity.

184

185 **Introducing ciliary ARL13B in 4-week-old *Arl13b*^{A/A} mice prevents obesity**

186 Ciliary ARL13B could control energy homeostasis through a role in development or in
187 adult mice. To address this, we induced expression of wildtype ARL13B, which localizes to cilia,
188 after development and tracked the body weight profile of the animals. We used a Cre-inducible
189 *Arl13b-Fucci2a* (AF2a) allele that expresses wildtype ARL13B fused to a Cerulean
190 fluorophore⁽³⁵⁾. We crossed *Arl13b*^{A/A};AF2a mice to *CAGG-CreER*^{T2} transgenic mice in which
191 Cre is ubiquitously activated following tamoxifen induction (**Figure 5A**). We confirmed that
192 ARL13B-Cerulean is present in cilia only after Cre recombination (**Figure 5 B and C**). ARL13B-
193 Cerulean co-localizes with the neuronal marker ADCY3 in the ARC, the PVN, and the VMH in
194 tamoxifen-treated *Arl13b*^{A/A};AF2a;*CAGG-CreER*^{T2} mice but not in tamoxifen-treated *Arl13b*^{A/A}
195 mice lacking Cre (**Supplemental Figure 3 A-F**).

196 We longitudinally tracked the impact of including ARL13B-Cerulean expression at 4-
197 weeks in *Arl13b*^{A/A};AF2a;*CAGG-CreER*^{T2} mice (referred to hereafter as *Arl13b*^{A/A};AF2a^{CAGG-4wk})
198 compared to controls *Arl13b*^{+/A};AF2a;*CAGG-CreER*^{T2} and *Arl13b*^{A/A} mice. From week 8 until
199 week 12, both male and female *Arl13b*^{A/A};AF2a^{CAGG-4wk} mice weighed significantly less than
200 *Arl13b*^{A/A} mice (**Figure 5 D and E**). These data demonstrate that ciliary ARL13B plays a role
201 after development is complete and suggest that ARL13B regulates acute signaling in cilia to
202 control body weight.

203 To examine the homeostatic response of *Arl13b*^{A/A};AF2a^{CAGG-4wk} mice to glucose and
204 insulin, we performed glucose and insulin tolerance tests in 13 to 15-week-old mice. In response
205 to glucose, male and female *Arl13b*^{A/A};AF2a^{CAGG-4wk} mice cleared glucose from their
206 bloodstream, similar to control mice, while *Arl13b*^{A/A} mice displayed elevated blood glucose
207 levels (**Figure 5 F and G**). In response to insulin, the blood glucose levels in male
208 *Arl13b*^{A/A};AF2a^{CAGG-4wk} mice trended with the levels in control animals (**Figure 5H**). In contrast,
209 insulin lowered blood glucose levels in female *Arl13b*^{A/A};AF2a^{CAGG-4wk} mice (**Figure 5I**). These
210 data demonstrate that introducing wildtype ARL13B in cilia of *Arl13b*^{A/A} mice normalizes

211 glycemic regulation, showing that ARL13B must be in cilia for normal glucose and insulin
212 metabolism.

213

214 **Discussion**

215 Our study identifies a cilia-specific role of ARL13B as a critical regulator of energy
216 homeostasis. Mice expressing the cilia-excluded variant, ARL13B^{V358A}, become hyperphagic,
217 obese, and insulin resistant soon after weaning. We also demonstrate that ARL13B's role in
218 energy homeostasis is independent of its GEF activity for ARL3. Finally, we show that the
219 obesity phenotype can be rescued by introducing ciliary ARL13B after weaning, demonstrating it
220 does not play a developmental role and suggesting ciliary ARL13B likely regulates energy
221 homeostasis via an acute signaling role in the adult. Together, these data reveal that ciliary
222 ARL13B is essential for food intake and body weight regulation in adult mice.

223 While ARL13B^{V358A} is an engineered mutation, we were surprised to observe obesity in
224 *Ar13b^{A/A}* mice as distinct patient mutations in *ARL13B* lead to JS^(10, 11). JS is clinically defined by
225 its neurodevelopmental features, including the diagnostic molar tooth structure on an MRI, as
226 well as developmental delay, breathing abnormalities, and abnormal eye movements; it is not
227 typically associated with obesity. Consistent with this, we did not observe a weight phenotype in
228 mice expressing the JS-causing variant, ARL13B^{R79Q}. It is notable that one JS patient with
229 obesity carried an ARL13B^{Y86C} mutation. However, it is not clear that the mutation caused the
230 obesity. The ARL13B^{Y86C} mutation, like ARL13B^{R79Q}, lacks GEF activity for ARL3. That said,
231 there are clear links between cilia and obesity^(36, 37). These include ciliopathies like BBS and
232 ALMS or mutations in the G-protein-coupled receptor melanocortin receptor 4 (MC4R), which
233 localizes to cilia^(38, 39). Thus, the cilia-specific role of ARL13B in controlling energy homeostasis
234 may involve interactions with other ciliopathy proteins or signaling machinery.

235 We conclude that ARL13B's GEF activity for ARL3 is unlikely to be required for energy
236 homeostasis. We base this on analysis of the ARL13B^{R79Q} mutation. The full-length,
237 recombinant mouse protein purified from HEK cells lacks any evidence of *in vitro* GEF activity
238 for ARL3⁽⁴⁾. It is worth noting that when a bacterially expressed, truncated protein that included
239 the homologous mutation (R77Q) in the Chlamydomonas ortholog of ARL13B, GEF activity
240 decreased compared to wild type, but residual activity was present⁽⁴⁰⁾. Reasons for this apparent
241 discrepancy (absent vs reduced GEF activity) could result from a number of differences,
242 including the use of mouse vs Chlamydomonas proteins (which share only 29.5% identity) or
243 the source of protein expression (mammalian vs bacterial). In any case, the analysis of the
244 mammalian protein directly reflects the consequences of this point mutation in mouse. It is
245 possible that the R79Q mutation disrupts additional ARL13B function. R79 plays an important
246 role in the conformational stability of ARL13B's switch II region, commonly used to bind
247 effectors. The mutation to glutamine (R79Q) in our mouse could alter binding not only to the
248 effector ARL3, for which it has GEF activity, but also to other unrecognized effectors. We also
249 cannot formally exclude the possibility of a compensatory GEF for ARL3 *in vivo*.

250 Given ARL13B's well-documented roles in development and the neural developmental
251 features of JS, we sought to determine whether ciliary ARL13B regulates developmental
252 processes. We first assessed whether there were developmental patterning phenotypes of the
253 hypothalamus that led to hyperphagia-associated obesity. Our analysis showed no overt
254 changes in cell population numbers within the ARC (POMC and AgRP). Additionally, we
255 induced expression of wild-type ARL13B-Cerulean at 4 weeks of age in *Arl13b^{AA}* mice and
256 observed a rescue of the obesity phenotype. Collectively, these data indicate that ciliary
257 ARL13B is not regulating developmental processes to control energy homeostasis and are
258 consistent with ciliary ARL13B controlling acute signaling in adult animals. While the ARL13B-
259 Cerulean induction was ubiquitous, we note that the hypothalamic circuits that control feeding

260 are established by four weeks of age, which is just prior to the significant weight gain we
261 observe in *Arl13b^{A/A}* mice⁽⁴¹⁾.

262 Our data clearly argue that obesity in *Arl13b^{A/A}* animals is driven by hyperphagia and
263 increased fat mass. The hyperphagic phenotype just before significant weight gain in *Arl13b^{A/A}*
264 mice strongly suggests the involvement of hypothalamic neurons. We observed that ARL13B is
265 normally in cilia on neurons in multiple hypothalamic feeding centers and on pancreatic islet
266 cells, but absent from cilia on these cell types in *Arl13b^{A/A}* mutants. We eliminated two
267 alternative possibilities for the weight phenotype. First, we previously reported
268 that *Arl13b^{A/A}* mice develop progressive, mild kidney cysts⁽²⁸⁾. However, the size and rate of
269 kidney cyst progression in these animals do not account for the changes in body weight and
270 composition we observe. Second, we showed that the weight phenotype does not depend on
271 gene dosage, as including the *Arl13b^{hnn}* null allele did not impact weight. Similarly, we found that
272 ARL13B overexpression using the inducible *Arl13b-Cerulean* allele did not impact weight⁽⁴²⁾.

273 One possible mechanism through which ciliary ARL13B regulates energy homeostasis
274 involves the established interaction between ARL13B and INPP5E in the ciliary membrane<sup>(6, 7,
275 32)</sup>. Patients lacking the C-terminal CaaX domain of INPP5E lose INPP5E ciliary localization and
276 exhibit MORM syndrome, which includes obesity⁽⁴³⁾. INPP5E is not detected in the cilia of
277 *Arl13b^{A/A}* cells, consistent with data showing that the ciliary retention of INPP5E depends on
278 ARL13B. Thus, the loss of ciliary INPP5E in the absence of ciliary ARL13B could impact the
279 trafficking or signaling of proteins implicated in feeding behavior, such as MC4R. This would
280 suggest the obesity-causing ARL13B^{V358A} mutation functions via INPP5E, whereas JS-causing
281 mutations in ARL13B act via ARL3. While a tantalizing model, it is challenging to reconcile with
282 *INPP5E* mutations causing JS or the finding that INPP5E requires activated ARL3 (ARL3-GTP)
283 to enter cilia.

284 Our *Arl13b*^{V358A} model isolates the ciliary role of the ARL13B protein. This model enables
285 us to directly interrogate, at a subcellular resolution, how ARL13B controls cilia-mediated
286 signaling pathways involved in maintaining energy homeostasis. A slight sex difference was
287 observed in the glucose homeostasis phenotype. This phenotype could be studied further once
288 the anatomical and cellular basis for ciliary *Arl13b*-dependent obesity has been identified. Our
289 data indicate that ARL13B typically localizes to cilia in tissues that regulate energy homeostasis.
290 The absence of ARL13B from cilia in these tissues leads to obesity, suggesting a critical role for
291 ciliary ARL13B in body weight control. Future studies will identify the cell type or combination of
292 cells that require ciliary ARL13B function and the mechanism of ciliary ARL13B action to
293 regulate energy homeostasis.

294

295 **Materials and Methods**

296 **Ethics Statement**

297 All mice were cared for in accordance with NIH guidelines, and animal experimental procedures
298 were approved by the Institutional Animal Care and Use Committees (IACUC) at Emory
299 University (20170058), the University of California, San Francisco (AN201856), and Indiana
300 University-Indianapolis (SC358R).

301 **Mouse lines.** Mice were housed in a barrier facility and maintained on a 12:12 light cycle (from
302 7 a.m. to 7 p.m.) at an ambient temperature of 23°C ± 2°C and relative humidity of 50%–70%.
303 Mice were fed with rodent diet 5058 (Lab Diet) and group housed (up to 5 mice per cage). Lines
304 used were *Arl13b*^{V358A} (C57BL/6J-*Arl13b*^{em1Tc}) [MGI: 6256969], *Arl13b*^{R79Q} (C57BL/6J-
305 *Arl13b*^{em2Tc}) [MGI: 6279301], and *Arl13b-Fucci2a* [MGI:6193732]⁽³⁵⁾. Mice were genotyped for
306 the V358A mutation using primers MB11: 5'-CCTATATTCTTCTAGAAAA-
307 CAGTAAGAAGAAAACCAAGAAACTAAGACTCCTTTCATTCATCGGGC-3' and MB12: 5'-

308 GACAGTAAAGGATTCTCCTCACACCTGAC-3' to detect the mutant allele, and primers
309 MB21: 5'-CTTAAGATGACTTGAGTTGGAAGAAATACAAGATAGC-3' and MB22: 5'-
310 GCGTGGGACTCTTGGAGTAGACTAGTCATAACAGACGGGTTCTA-3' to detect the wildtype
311 allele. Band sizes were 395bp for wildtype and 273bp for mutant. Mice were genotyped for the
312 R79Q mutation using primers 223_2F: 5'-TCACTTGCAACAGAGCATCC-3' and 223_2R: 5'-
313 ACAGCTCTGCCGTGTTAC-3' followed by Sanger sequencing the 304bp PCR product. Mice
314 were genotyped for the *Arl13b-Fucci2a* allele using primers F: 5'- AAAACCTCCCACACCTCCC
315 -3' and R: 5'- CGACCATCACAAAGTGTCAACC -3'.

316 **Mouse metabolism studies.** Mice were single-housed for 7 days, and food was weighed daily.
317 The average daily food weight between groups was taken. Energy expenditure was measured
318 by the Comprehensive Lab Animal Monitoring System (CLAMS, Columbus Instruments,
319 Columbus, Ohio). Mice were tested over 96 continuous hours, and the data from the last 48
320 hours were analyzed. Kilocalories per hour were calculated using the Lusk equation: Energy
321 Expenditure = (3.815 + 1.232 × respiratory exchange ratio [RER]) × oxygen consumption rate
322 (VO₂) and analyzed with CalR software⁽⁴⁴⁾ (ANCOVA with body weight used as a covariate).
323 Lean mass and fat mass were measured using the EchoMRITM system⁽⁴⁵⁾.

324 **Glucose tolerance test.** Adult mice were fasted for 16 hours and injected with 1 g/kg body
325 weight glucose intraperitoneally (Sigma G7021). Blood glucose was measured at 0, 10, 20, 30,
326 60, 90, and 120 minutes via tail sampling with the AlphaTrak3 blood glucose meter (Zoetis). A
327 blood sample for fasting glucose levels was taken at time point 0, before glucose was injected.

328 **Insulin tolerance test.** Adult mice were fasted for 3 hours before intraperitoneal injection with
329 0.75 U/kg body weight regular human insulin (Humulin R, Lilly USA, and Novolin R, Novo
330 Nordisk). Blood glucose levels were measured at 0, 15, 30, 45, and 60 minutes. A blood sample
331 for fasting insulin levels was taken at time point 0, before insulin was administered.

332 **Blood serum analysis.** Blood was allowed to coagulate at room temperature for 30 minutes,
333 then centrifuged at 1200 x g for 10 min at room temperature. Serum was collected and stored at
334 -80°C. Insulin and leptin levels were measured with Crystal Chem's ultra-sensitive mouse
335 ELISA kits according to the manufacturer's protocol (leptin: catalog # 90080 and insulin catalog
336 # 90030).

337 **Tamoxifen administration.** Tamoxifen (Sigma T5648) stock solution was prepared at a
338 concentration of 20mg/ml in 100% EtOH and stored at -20°C. Each dose of tamoxifen was
339 freshly prepared in corn oil on the day of injection and dissolved using a speed vacuum
340 centrifuge (Eppendorf Vacufuge plus). To induce gene expression, 10ul/g tamoxifen in 200ul
341 corn oil was administered by oral gavage to 4-week-old mice using a 1ml syringe and a 22G
342 1.5-inch straight needle (Braintree Scientific Inc).

343 **Tissue harvesting and preparation.** Mice were euthanized with isoflurane inhalation followed
344 by perfusion with ice-cold PBS and ice-cold 4% paraformaldehyde (PFA). Brain and pancreas
345 tissues were harvested and post-fixed with 4% PFA overnight at 4°C. Tissues were then
346 cryoprotected in 30% sucrose in 0.1 M phosphate buffer at 4°C until tissues sank in solution.
347 Samples were then frozen in optimal cutting temperature compound (Tissue-Tek OCT, Sakura
348 Finetek).

349 **Immunohistochemistry.** 12µm or 20µm cryosections were rehydrated, blocked and
350 permeabilized in antibody wash (5% heat-inactivated goat serum, 0.1% Triton X-100 in Tris-
351 buffered Saline) for 30-40 minutes. Tissues were incubated with primary antibodies overnight at
352 4°C, washed three times with 0.1% Triton X-100 in Tris-Buffered Saline (TBST), and incubated
353 with secondary antibodies for 1 hour at room temperature. Tissues were washed three times
354 with TBST and incubated with Hoechst 33342 for 5 minutes. Slides were coverslipped with
355 ProLong Gold (ThermoFisher) mounting media. Slides cured overnight at room temperature in
356 the dark and were stored long-term at -20°C. Slides were imaged on a BioTek Lionheart FX

357 microscope. Primary antibodies used were: mouse anti-ARL13B (1:1000, NeuroMab,
358 N295B/66); rabbit anti-acetylated α -tubulin (1:1000, Cell Signaling, 5335); mouse anti-acetylated
359 α -tubulin (1:2500, Sigma, T7451); chicken anti-ACIII (1:1000, Encor, CPC-A-ACIII); rat anti-
360 insulin (1:1000, R&D systems, MAB1417); rabbit anti-glucagon (1:2000, Abcam, ab92517),
361 chicken anti-GFP (1:8000, Abcam, ab13970) recognizes cerulean. Secondary antibodies used
362 were goat anti-mouse AlexaFluor 488, goat anti-chicken AlexaFluor 647, goat anti-chicken
363 AlexaFluor 488, goat anti-rat AlexaFluor 568 and donkey anti-rabbit AlexaFluor 555 (all at
364 1:500, ThermoFisher).

365 **RNAScope.** Brains from adult mice were harvested, fixed, and prepared for RNAscope in situ
366 hybridization^(46, 47). Briefly, 15 μ m cryosections were mounted on slides and then post-fixed with
367 4% PFA for 16hr at 4°C. Detection of transcripts was performed using the RNAscope 2.5 HD
368 Duplex Assay (Advanced Cell Diagnostics (ACD), Newark, CA). Tissue pretreatment was
369 performed according to technical note 320534 Rev A. Probe hybridization, counterstaining, and
370 mounting of slides were performed according to user manual no. 322500-USM Rev A. Slides
371 were assayed using probes to AgRP (Cat No. 400711) and POMC (Cat No. 314081) transcripts
372 (ACD). Sections were counterstained with hematoxylin, dehydrated, and mounted using
373 VectaMount (Vectorlabs, Burlingame, CA). Slides with positive control probe (PPIB-
374 C1/POLR2A-C2; Cat No. 321651) and negative control probe (DapB; Cat No. 320751) were run
375 with each experiment. (n \geq 3 animals per group).

376

377 **Funding**

378 This work was supported by the National Institutes of Health: diversity supplement to
379 R35GM122549 and F32DK137409 (TTT); T32NS096050, diversity supplement to
380 R01NS090029 and F31NS106755 (EDG); Larry L. Hillblom Foundation fellowship (CMA);

381 University Fellowship and F31DK142351 (KMB); American Heart Association pre-doctoral
382 fellowship (XY); R01DK114008 (NFB); R01DK124769, R01DK106404 and R01DK060540 (CV);
383 and R01NS090029, R35GM122549 and R35GM148416 (TC).

384

385 **Reference List**

386

387 1. Larkins CE, Gonzalez Aviles GD, East MP, Kahn RA, Caspary T. Arl13b regulates
388 ciliogenesis and the dynamic localization of Shh signaling proteins. *Molecular Biology of*
389 *the Cell*. 2011;22(23):4694-703.

390 2. Sun Z, Amsterdam A, Pazour GJ, Cole DG, Miller MS, Hopkins N. A genetic
391 screen in zebrafish identifies cilia genes as a principal cause of cystic kidney.
392 *Development*. 2004;131(16):4085-93.

393 3. Gotthardt K, Lokaj M, Koerner C, Falk N, Gießl A, Wittinghofer A. A G-protein
394 activation cascade from Arl13B to Arl3 and implications for ciliary targeting of lipidated
395 proteins. *eLife*. 2015;4:1-16.

396 4. Ivanova AA, Caspary T, Seyfried NT, Duong DM, West AB, Liu Z, et al.
397 Biochemical characterization of purified mammalian ARL13B protein indicates that it is
398 an atypical GTPase and ARL3 guanine nucleotide exchange factor (GEF). *Journal of*
399 *Biological Chemistry*. 2017;292(26):11091-108.

400 5. Nozaki S, Katoh Y, Terada M, Michisaka S, Funabashi T, Takahashi S, et al.
401 Regulation of ciliary retrograde protein trafficking by the Joubert syndrome proteins
402 ARL13B and INPP5E. *Journal of Cell Science*. 2017;130(3):563-76.

403 6. Humbert MC, Weihbrecht K, Searby CC, Li Y, Pope RM, Sheffield VC, et al.
404 ARL13B, PDE6D, and CEP164 form a functional network for INPP5E ciliary targeting.
405 *Proceedings of the National Academy of Sciences of the United States of America*.
406 2012;109(48):19691-6.

407 7. Qiu H, Fujisawa S, Nozaki S, Katoh Y, Nakayama K. Interaction of INPP5E with
408 ARL13B is essential for its ciliary membrane retention but dispensable for its ciliary
409 entry. *Biology Open*. 2021;10(1).

410 8. Caspary T, Larkins CE, Anderson KV. The Graded Response to Sonic Hedgehog
411 Depends on Cilia Architecture. *Developmental Cell*. 2007;12(5):767-78.

412 9. Su CY, Bay SN, Mariani LE, Hillman MJ, Caspary T. Temporal deletion of Arl13b
413 reveals that a mispatterned neural tube corrects cell fate over time. *Development*
414 (Cambridge). 2012;139(21):4062-71.

415 10. Cantagrel V, Silhavy JL, Bielas SL, Swistun D, Marsh SE, Bertrand JY, et al.
416 Mutations in the Cilia Gene ARL13B Lead to the Classical Form of Joubert Syndrome.
417 *American Journal of Human Genetics*. 2008;83(2):170-9.

418 11. Thomas S, Cantagrel V, Mariani L, Serre V, Lee JE, Elkhartoufi N, et al.
419 Identification of a novel ARL13B variant in a Joubert syndrome-affected patient with
420 retinal impairment and obesity. *European Journal of Human Genetics*. 2015;23(5):621-
421 7.

422 12. Gigante ED, Taylor MR, Ivanova AA, Kahn RA, Caspary T. ARL13B regulates
423 Sonic Hedgehog signaling from outside primary cilia. *bioRxiv*. 2019:1-23.

424 13. Collin GB, Marshall JD, Ikeda A, So WV, Russell-Eggitt I, Maffei P, et al.
425 Mutations in ALMS1 cause obesity, type 2 diabetes and neurosensory degeneration in
426 Alström syndrome. *Nature Genetics*. 2002;31(1):74-8.

427 14. Forsythe E, Beales PL. Bardet-Biedl syndrome. *European Journal of Human
428 Genetics*. 2013;21(1):8-13.

429 15. Hearn T, Spalluto C, Phillips VJ, Renforth GL, Copin N, Hanley NA, et al.
430 Subcellular Localization of ALMS1 Supports Involvement of Centrosome and Basal
431 Body Dysfunction in the Pathogenesis of Obesity, Insulin Resistance, and Type 2
432 Diabetes. *Electrophoresis*. 2005;54(May):1581-7.

433 16. Collin GB, Cyr E, Bronson R, Marshall JD, Gifford EJ, Hicks W, et al. Alms1-
434 disrupted mice recapitulate human Alström syndrome. *Human Molecular Genetics*.
435 2005;14(16):2323-33.

436 17. Arsov T, Silva DG, O'Bryan MK, Sainsbury A, Lee NJ, Kennedy C, et al. Fat
437 aussie - A new Alström syndrome mouse showing a critical role for ALMS1 in obesity,
438 diabetes, and spermatogenesis. *Molecular Endocrinology*. 2006;20(7):1610-22.

439 18. Heydet D, Chen LX, Larter CZ, Inglis C, Silverman MA, Farrell GC, et al. A
440 truncating mutation of Alms1 reduces the number of hypothalamic neuronal cilia in
441 obese mice. *Developmental Neurobiology*. 2013;73(1):1-13.

442 19. Berbari NF, Lewis JS, Bishop GA, Askwith CC, Mykytyn K. Bardet-Biedl
443 syndrome proteins are required for the localization of G protein-coupled receptors to
444 primary cilia. 2008.

445 20. Domire JS, Green JA, Lee KG, Johnson AD, Askwith CC, Mykytyn K. Dopamine
446 receptor 1 localizes to neuronal cilia in a dynamic process that requires the Bardet-Biedl
447 syndrome proteins. *Cellular and Molecular Life Sciences*. 2011;68(17):2951-60.

448 21. Shinde SR, Nager AR, Nachury MV. Ubiquitin chains earmark GPCRs for
449 BBSome-mediated removal from cilia. *Journal of Cell Biology*. 2020;219(12).

450 22. Ye F, Nager AR, Nachury MV. BBSome trains remove activated GPCRs from cilia
451 by enabling passage through the transition zone. *Journal of Cell Biology*.
452 2018;217(5):1847-68.

453 23. Davenport JR, Watts AJ, Roper VC, Croyle MJ, van Groen T, Wyss JM, et al.
454 Disruption of Intraflagellar Transport in Adult Mice Leads to Obesity and Slow-Onset
455 Cystic Kidney Disease. *Current Biology*. 2007;17(18):1586-94.

456 24. Berbari NF, Pasek RC, Malarkey EB, Yazdi SMZ, McNair AD, Lewis WR, et al.
457 Leptin resistance is a secondary consequence of the obesity in ciliopathy mutant mice.

458 Proceedings of the National Academy of Sciences of the United States of America.
459 2013;110(19):7796-801.

460 25. Wang Y, Bernard A, Comblain F, Yue X, Paillart C, Zhang S, et al. Melanocortin 4
461 receptor signals at the neuronal primary cilium to control food intake and body weight.
462 *Journal of Clinical Investigation*. 2021;131(9).

463 26. Wang L, De Solis AJ, Goffer Y, Birkenbach KE, Engle SE, Tanis R, et al. Ciliary
464 gene RPGRIP1L is required for hypothalamic arcuate neuron development. *JCI Insight*.
465 2019;4(3).

466 27. Mariani LE, Bijlsma MF, Ivanova AI, Suciu SK, Kahn RA, Caspary T. Arl13b
467 regulates Shh signaling from both inside and outside the cilium. *Molecular Biology of the*
468 *Cell*. 2016;27(23):3780-90.

469 28. Van Sciver RE, Long AB, Katz HG, Gigante ED, Caspary T. Ciliary ARL13B
470 inhibits developmental kidney cystogenesis in mouse. *Developmental Biology*.
471 2023;500:1-9.

472 29. Brewer KM, Brewer KK, Richardson NC, Berbari NF. Neuronal cilia in energy
473 homeostasis. *Frontiers in Cell and Developmental Biology*: Frontiers Media S.A.; 2022.

474 30. Bishop GA, Berbari NF, Lewis J, Mykytyn K. Type III adenylyl cyclase localizes to
475 primary cilia throughout the adult mouse brain. *Journal of Comparative Neurology*.
476 2007;505(5):562-71.

477 31. De Solis AJ, Del Río-Martín A, Radermacher J, Chen W, Steuernagel L, Bauder
478 CA, et al. Reciprocal activity of AgRP and POMC neurons governs coordinated control
479 of feeding and metabolism. *Nature Metabolism*. 2024;6(3):473-93.

480 32. Fujisawa S, Qiu H, Nozaki S, Chiba S, Katoh Y, Nakayama K. ARL3 and ARL13B
481 GTPases participate in distinct steps of INPP5E targeting to the ciliary membrane.
482 *Biology Open*. 2021;10(9).

483 33. Zhang Q, Li Y, Zhang Y, Torres VE, Harris PC, Ling K, et al. GTP-binding of ARL-
484 3 is activated by ARL-13 as a GEF and stabilized by UNC-119. *Scientific Reports*.
485 2016;6.

486 34. Suciu SK, Long AB, Caspary T. Smoothened and ARL13B are critical in mouse
487 for superior cerebellar peduncle targeting. *Genetics*. 2021;218(4).

488 35. Ford MJ, Yeyati PL, Mali GR, Keighren MA, Waddell SH, Mjoseng HK, et al. A
489 Cell/Cilia Cycle Biosensor for Single-Cell Kinetics Reveals Persistence of Cilia after
490 G1/S Transition Is a General Property in Cells and Mice. *Developmental Cell*.
491 2018;47(4):509-23.e5.

492 36. Vaisse C, Reiter JF, Berbari NF. Cilia and obesity. *Cold Spring Harbor*
493 *Perspectives in Biology*. 2017;9(7).

494 37. Engle SE, Bansal R, Antonellis PJ, Berbari NF. Cilia signaling and obesity.
495 *Seminars in Cell and Developmental Biology*: Elsevier Ltd; 2021. p. 43-50.

496 38. Siljee JE, Wang Y, Bernard AA, Ersoy BA, Zhang S, Marley A, et al. Subcellular
497 localization of MC4R with ADCY3 at neuronal primary cilia underlies a common pathway
498 for genetic predisposition to obesity. *Nature Genetics*. 2018;50(2):180-5.

499 39. Vaisse C, Clement K, Durand E, Hercberg S, Guy-Grand B, Froguel P.
500 Melanocortin-4 receptor mutations are a frequent and heterogeneous cause of morbid
501 obesity. *The Journal of Clinical Investigation*. 2000;106(2):253-62.

502 40. Miertzschke M, Koerner C, Spoerner M, Wittinghofer A. Structural insights into
503 the small G-protein Arl13B and implications for Joubert syndrome. *Biochem J*.
504 2014;457(2):301-11.

505 41. Bouret SG. Developmental programming of hypothalamic melanocortin circuits.
506 *Experimental and Molecular Medicine*. 2022;54:403-13.

507 42. Long AB, Wilson IM, Terry TT, Van Sciver RE, Caspary T. ARL13B-Cerulean
508 rescues Arl13b-null mouse from embryonic lethality and reveals a role for ARL13B in
509 spermatogenesis. 2025.

510 43. Jacoby M, Cox JJ, Gayral S, Hampshire DJ, Ayub M, Blockmans M, et al.
511 INPP5E mutations cause primary cilium signaling defects, ciliary instability and
512 ciliopathies in human and mouse. *Nature Genetics*. 2009;41(9):1027-31.

513 44. Mina AI, LeClair RA, LeClair KB, Cohen DE, Lantier L, Banks AS. CalR: A Web-
514 Based Analysis Tool for Indirect Calorimetry Experiments. *Cell Metabolism*.
515 2018;28(4):656-66.e1.

516 45. Jones AS, Johnson MS, Nagy TR. Validation of quantitative magnetic resonance
517 for the determination of body composition of mice. *International Journal of Body
518 Composition Research*. 2009;7(2):67-72.

519 46. Antonellis PJ, Engle SE, Brewer KM, Berbari NF. The hedgehog signaling
520 pathway is expressed in the adult mouse hypothalamus and modulated by fasting.
521 *eNeuro*. 2021;8(5).

522 47. Engle SE, Antonellis PJ, Whitehouse LS, Bansal R, Emond MR, Jontes JD, et al.
523 A CreER mouse to study melanin concentrating hormone signaling in the developing
524 brain. *Genesis*. 2018;56(8):1-7.

525

526

527 **Figure Legends**

528 **Figure 1: *ARL13B*^{V358A} protein is undetectable in primary cilia in adult mouse tissues.**

529 **(A)** Schematic of ARL13B protein domains and relevant amino acid sequence in wildtype and
530 mutant in the cilia localization sequence (CLS). **(B)** Schematic of ARL13B (green) localization in

531 a wildtype (*Arl13b*^{+/+}), (grey) null (*Arl13b*^{hnn/hnn}), and cilia-excluded (*Arl13b*^{A/A}) models. (C-H)
532 Immunofluorescence of ADCY3 (red) and ARL13B (green) in hypothalamic feeding centers PVN
533 (C-D), VMH (E-F), ARC (G-H) in the mouse brain from *Arl13b*^{+/+} controls and *Arl13b*^{A/A} mice.
534 Scale bars 20 μ m and 5 μ m for insets indicated by white boxes. Hoechst-stained nuclei are blue.

535

536 **Figure 2: Exclusion of ARL13B from cilia leads to obesity.**

537 (A-B) Weekly male and female body weights from 3 to 10 weeks of age: *Arl13b*^{+/+} (males n=14;
538 females n=13), *Arl13b*^{A/A} (males n=22; females n=22), *Arl13b*^{hnn/hnn} (males n=10; females n=9),
539 *Arl13b*^{A/A} (males n=24; females n=26), and *Arl13b*^{A/hnn} (males n=15; females n=17). Data are
540 presented as means \pm SD. *P* values were determined by repeated measures ANOVA with
541 Tukey's multiple comparisons test. **P* \leq 0.01. (C and H) Lean mass and (D and I) fat mass of
542 male and female control (*Arl13b*^{+/+}) and *Arl13b*^{A/A}. (E and J) Serum leptin levels. (F and K) Food
543 intake. (G and L) Energy expenditure. Data are presented as means \pm SD. N numbers indicated
544 on graphs. Lean mass, fat mass, serum leptin, and food intake were analyzed using the Mann-
545 Whitney U test. Energy Expenditure was analyzed by CalR ANCOVA, with body weight included
546 as a covariate. ***P* $<$ 0.01; ****P* $<$ 0.001; ns, not significant with *P* $>$ 0.05.

547

548 **Figure 3: Insulin resistance and impaired glucose metabolism in *Arl13b*^{A/A} mice**

549 (A-B) Serum insulin levels in nonfasted 10-week-old male and female mice. Data points
550 represent individual mice. Data are presented as means \pm SD. Serum levels were analyzed
551 using the Mann-Whitney U test. **P* \leq 0.05; ***P* \leq 0.01. (C-D) Glucose tolerance test in males
552 and females. Blood glucose was measured at indicated times after i.p. glucose injection. (E-F)
553 Insulin tolerance test of males and females. Blood glucose was measured at indicated times
554 after i.p. insulin injection. The control group comprised pooled data from *Arl13b*^{+/+}, *Arl13b*^{A/A}, and

555 *Arl13b*^{+/hnn} mice, and they did not differ in body weight. Data are presented as means \pm SD. N
556 numbers indicated on graphs. *P* values were determined by repeated measures ANOVA with
557 Sidak's multiple comparisons test. **P* \leq 0.05; ***P* \leq 0.01, ****P* \leq 0.001; *****P* \leq 0.0001; ns, not
558 significant with *P* $>$ 0.05.

559

560 **Figure 4: ARL13B's GEF activity for ARL3 is not required for energy homeostasis.**

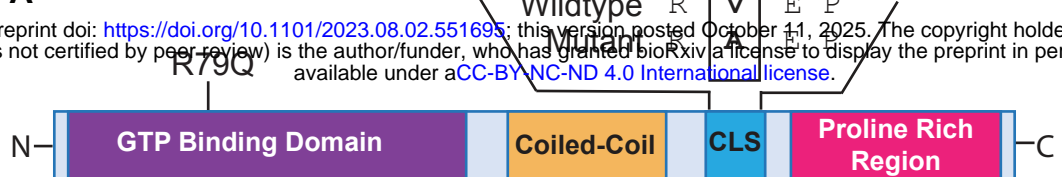
561 (A-B) Body weights of adult male and female controls (*Arl13b*^{+/+}) and mutants (*Arl13b*^{R79Q/R79Q}).
562 Data are presented as means \pm SD. N numbers indicated on graphs. ns, not significant with
563 Mann Whitney U test indicating *P* $>$ 0.05.

564

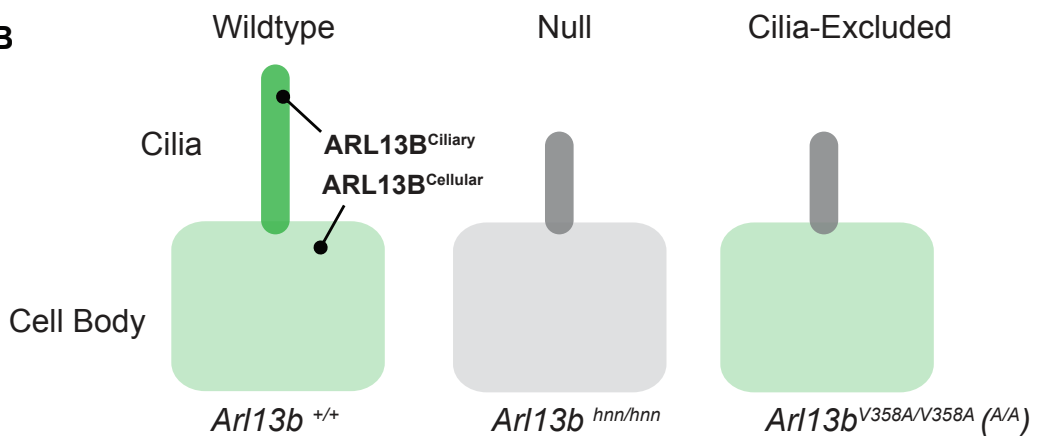
565 **Figure 5: Rescuing ciliary expression of ARL13B in adult mice prevents the metabolic**
566 **phenotype of *Arl13b*^{A/A} mice.**

567 (A) Schematic of the *Arl13b-Fucci2a* conditional allele with tamoxifen Cre induction timeline. (B-
568 C) Immunofluorescence of ADCY3 (red) and cerulean (cyan). (B) without Cre recombination.
569 (C) with Cre-recombination. (D-E) Longitudinal body weight data of control, *Arl13b*^{A/A}, and
570 Rescue (*Arl13b*^{A/A}; *AF2a*; *CAGG-CreER*^{T2}). Data are presented as means \pm SD. N numbers
571 indicated on graphs. *P* values were determined by repeated measures ANOVA with Tukey's
572 multiple comparisons test. **P* \leq 0.01. (F-G) Glucose tolerance test in males and females. Blood
573 glucose was measured at indicated times after i.p. glucose injection. (H-I) Insulin tolerance test
574 in males and females. Blood glucose was measured at indicated times after i.p. insulin injection.
575 N numbers indicated on graphs. Data are presented as means \pm SD. *P* values were determined
576 by repeated measures ANOVA with Tukey's multiple comparisons test. **P* \leq 0.05; ***P* \leq 0.01;
577 ****P* \leq 0.001; ns, not significant with *P* $>$ 0.05.

A

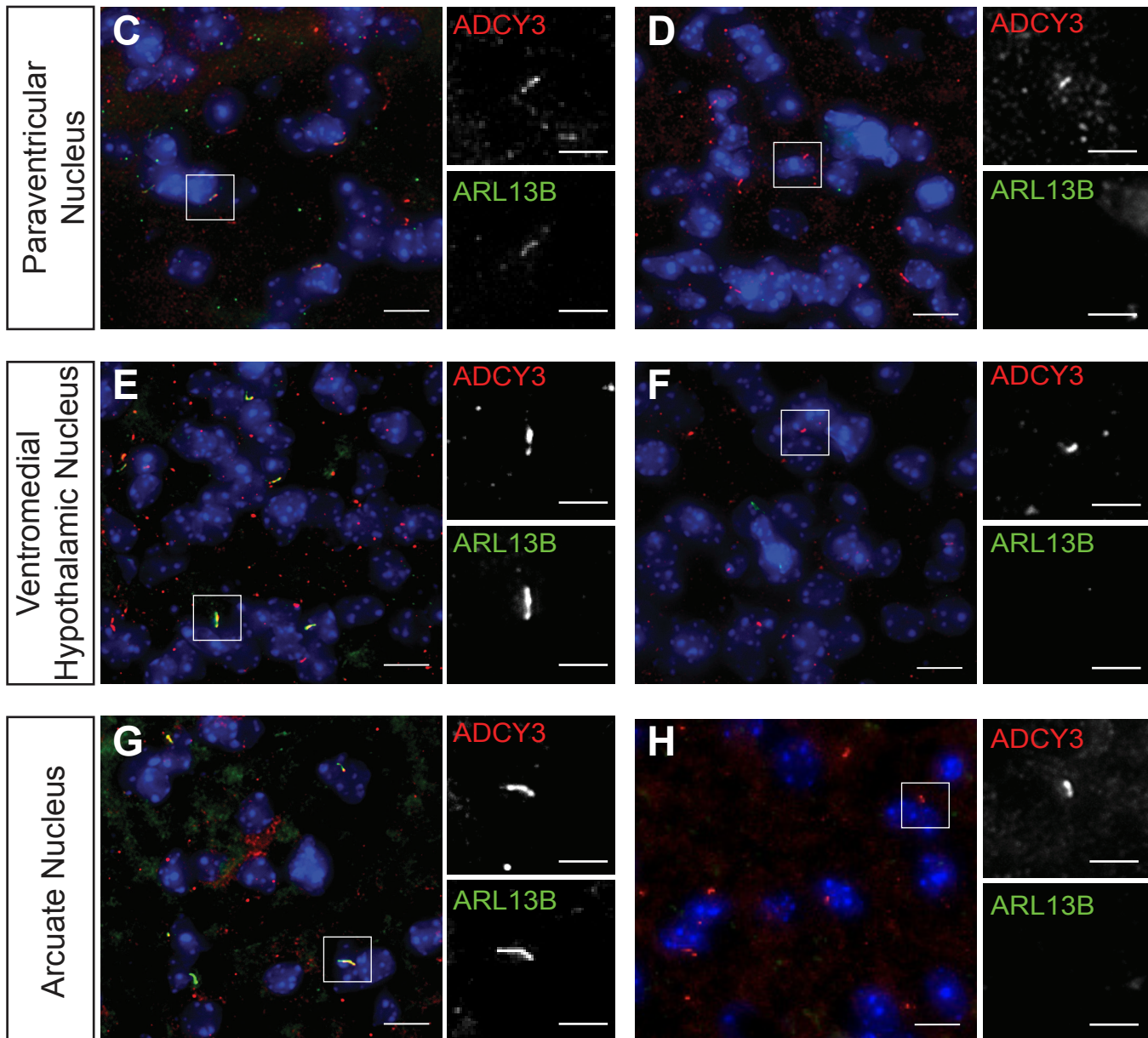


B



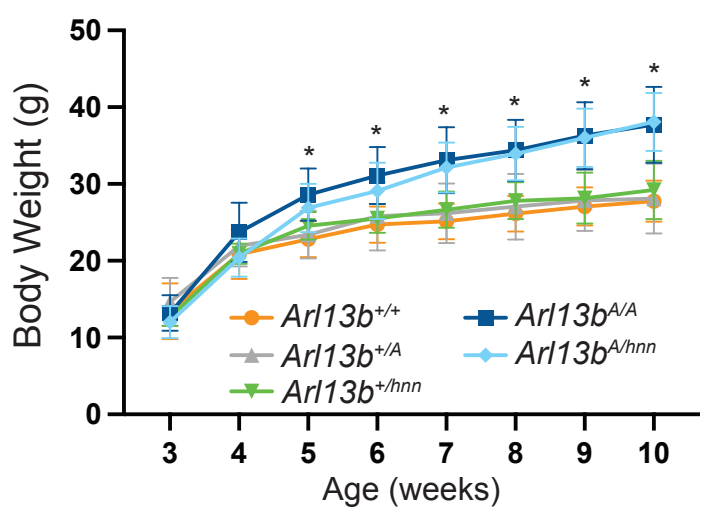
Arl13b^{+/+}

Arl13b^{A/A}



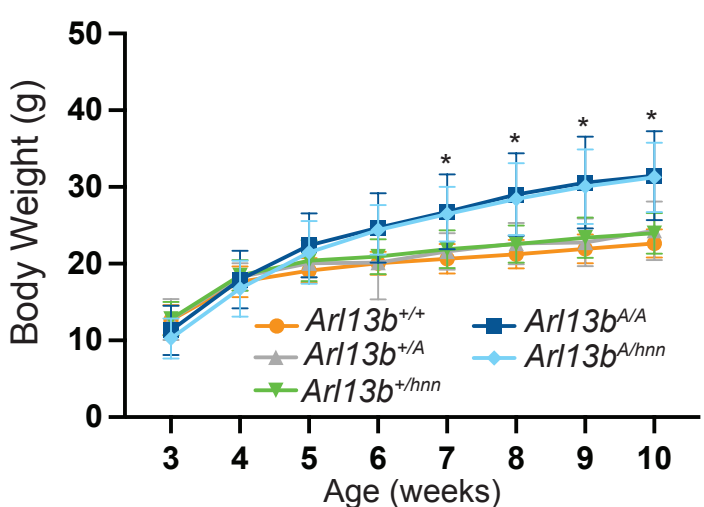
A

Males

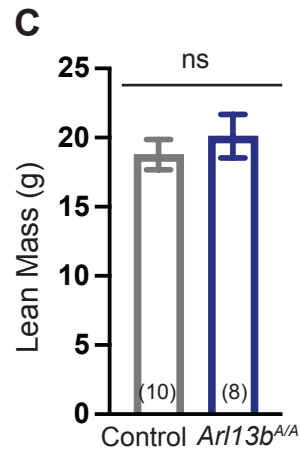


B

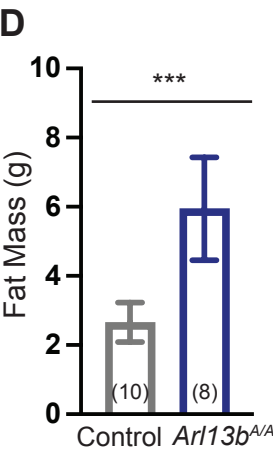
Females



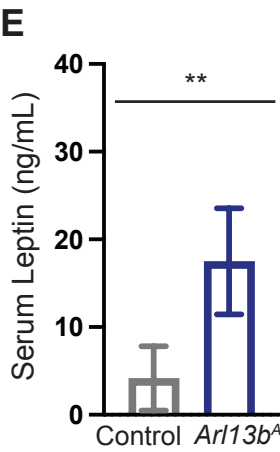
Males



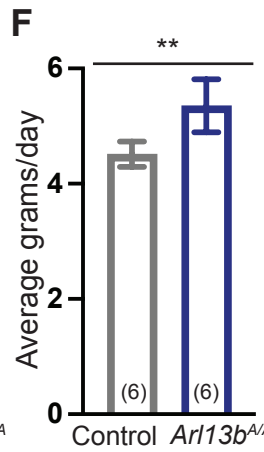
D



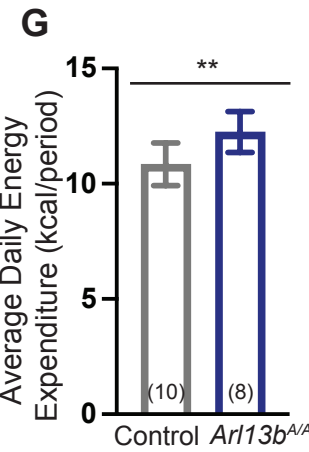
E



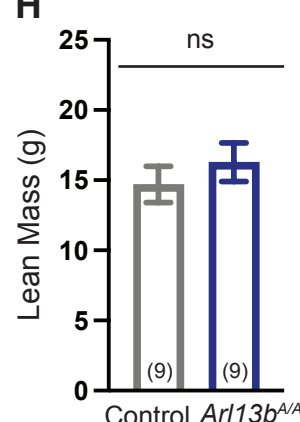
F



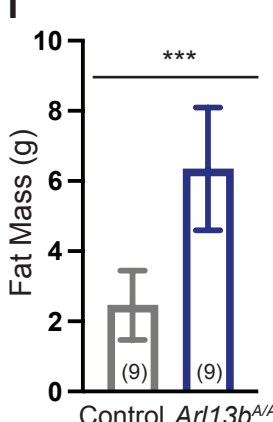
G



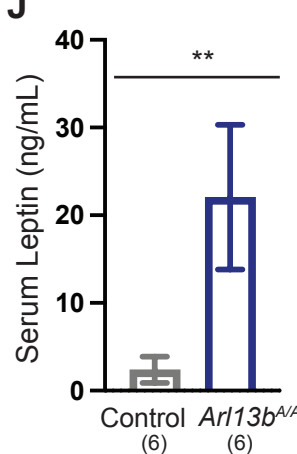
Females



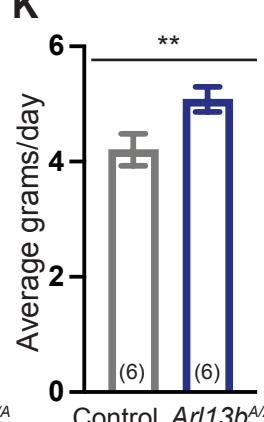
I



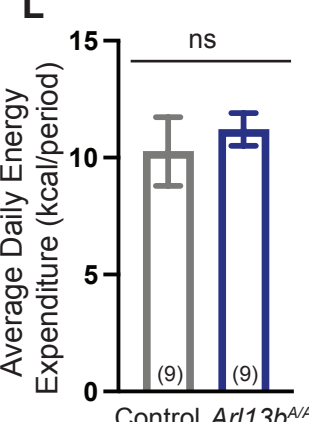
J

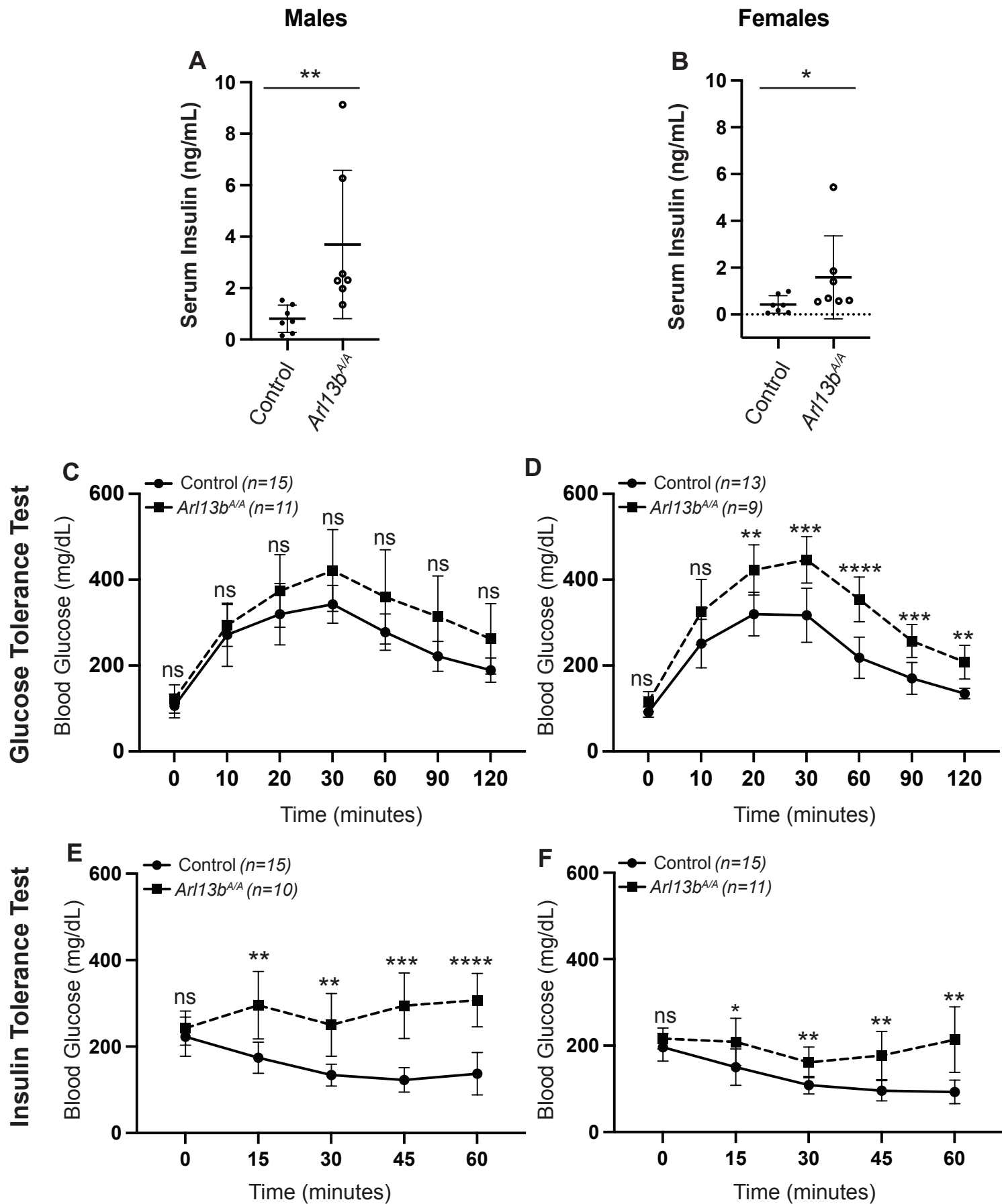


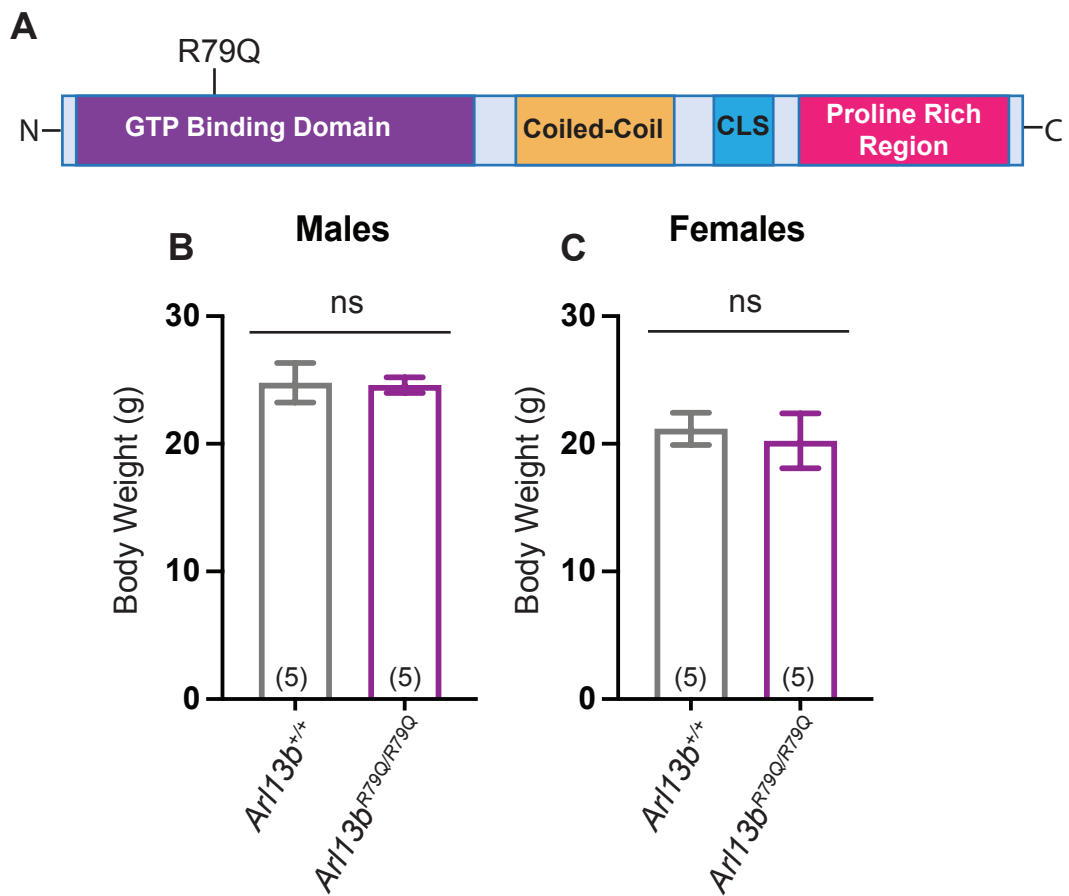
K



L

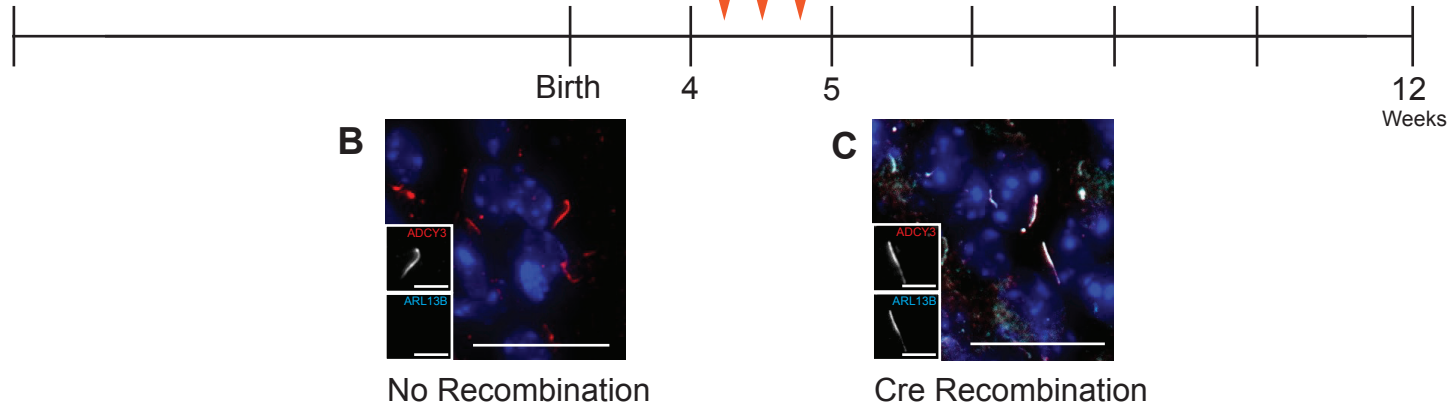
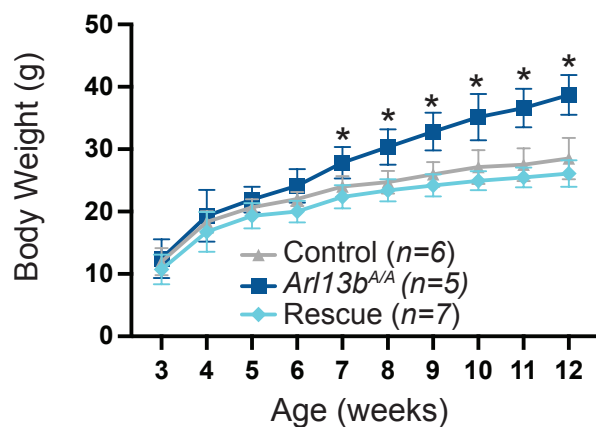
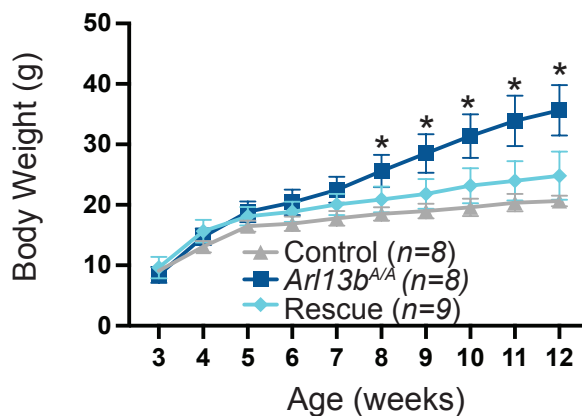
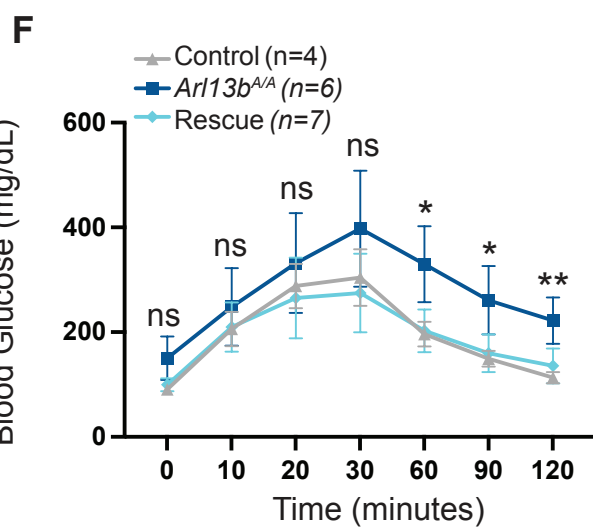
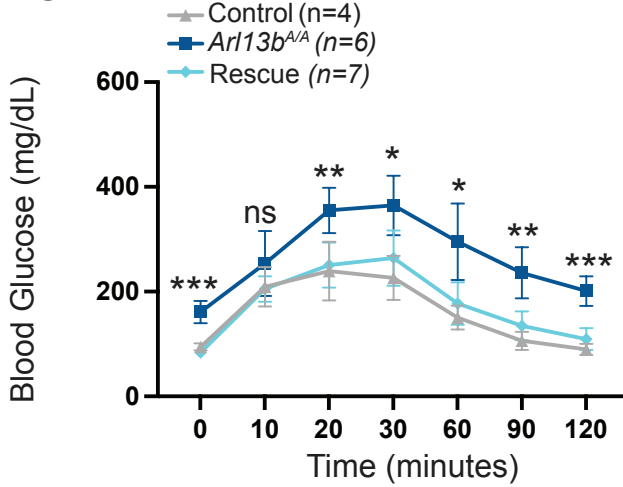
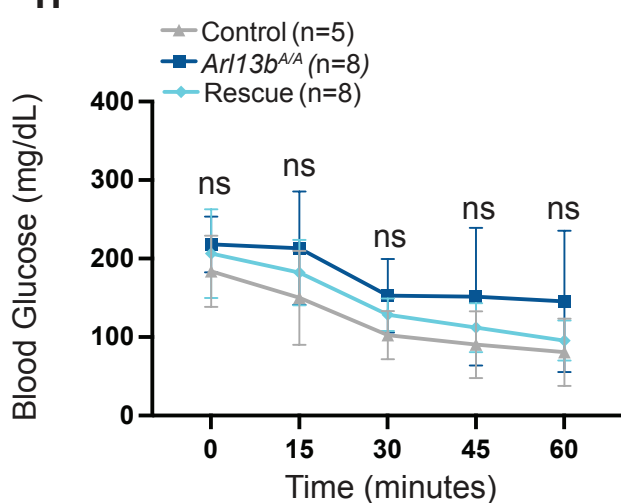






A

CAG bioRxiv preprint doi: <https://doi.org/10.1101/2018.08.02.251695>; this version posted October 14, 2018. The copyright holder for this preprint (which was not certified by peer review) is the author/funder, who has granted bioRxiv a license to display the preprint in perpetuity. It is made available under aCC-BY-NC-ND 4.0 International license.

**D****Males****E****Females****Glucose Tolerance Test****G****Insulin Tolerance Test****I**